Journal of Advanced Research (2016) 7, 113–124

Cairo University

Journal of Advanced Research

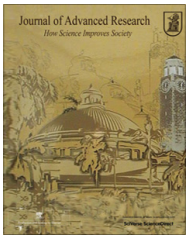

ORIGINAL ARTICLE

Adsorption of Methylene Blue, Bromophenol Blue, and Coomassie Brilliant Blue by α-chitin nanoparticles

Solairaj Dhananasekaran [a], **Rameshthangam Palanivel** [a,*], **Srinivasan Pappu** [b]

[a] *Department of Biotechnology, DDE, Science Campus, Alagappa University, Karaikudi, Tamil Nadu 630 004, India*
[b] *Department of Bioinformatics, Science Campus, Alagappa University, Karaikudi, Tamil Nadu 630 004, India*

ARTICLE INFO

Article history:
Received 4 January 2015
Received in revised form 10 March 2015
Accepted 25 March 2015
Available online 16 May 2015

Keywords:
Chitin nanoparticles
Methylene Blue
Bromophenol Blue
Coomassie Brilliant Blue
Penaeus monodon (Fabricius, 1798)

ABSTRACT

Expelling of dyestuff into water resource system causes major thread to the environment. Adsorption is the cost effective and potential method to remove the dyes from the effluents. Therefore, an attempt was made to study the adsorption of dyestuff (Methylene Blue (MB), Bromophenol Blue (BPB) and Coomassie Brilliant Blue (CBB)) by α-chitin nanoparticles (CNP) prepared from *Penaeus monodon* (Fabricius, 1798) shell waste. On contrary to the most recognizable adsorption studies using chitin, this is the first study using unique nanoparticles of ⩽50 nm used for the dye adsorption process. The results showed that the adsorption process increased with increase in the concentration of CNP, contact time and temperature with the dyestuff, whereas the adsorption process decreased with increase in the initial dye concentration and strong acidic pH. The results from Fourier transform infrared (FTIR) spectroscopy confirmed that the interaction between dyestuff and CNP involved physical adsorption. The adsorption process obeys Langmuir isotherm (R^2 values were 0.992, 0.999 and 0.992 for MB, BPB and CBB, and R_L value lies between 0 and 1 for all the three dyes) and pseudo second order kinetics (R^2 values were 0.996, 0.999 and 0.996 for MB, BPB and CBB) more effectively. The isotherm and kinetic models confirmed that CNP can be used as a suitable adsorbent material for the removal of dyestuff from effluents.

Introduction

Effluents from various industries contain harmful coloring agents, which have to be removed to maintain the quality of the environment. Paper, fabric, leather and dyestuff production are some of the industries that release harmful effluents [1]. Dyes used in various industries have harmful effects on living organisms within short exposure periods. The disposal of dyes in wastewater is an environmental problem that causes ill effects

* Corresponding author. Tel.: +91 9444834424; fax: +91 4565225216.
E-mail addresses: rameshthangam@alagappauniversity.ac.in, rameshthangam@gmail.com (R. Palanivel).

Peer review under responsibility of Cairo University.

Production and hosting by Elsevier

http://dx.doi.org/10.1016/j.jare.2015.03.003
2090-1232

to the ecosystem [2]. Conventional wastewater treatments such as chemical coagulation, activated sludge, trickling filter, carbon adsorption and photo-degradation were used for the removal of dyes [3]. Recently adsorption processes have been demonstrated as a potential technique for the removal of dyes from wastewater. Dye adsorption is a process of transfer of dye molecules from bulk solution phase to the surface of the adsorbent. Screening of biological adsorbents is an eventual task for environmental scientists and engineers, with its due merits. The most common biological adsorbents, or material from which they are produced, used in the process of adsorption include activated carbon (coconut shell), tree bark, lignin, shellfish shells, cotton, zeolites, fern, and compounds contained in a number of minerals and microorganisms (bacteria, fungi and yeast) [4]. Ease of access, cheap rate, reliability and ability to compete favorably with the conventional adsorbents make the biological adsorbents on demand than the synthetic ones [5].

Chitin is a biopolymer of 2-deoxy-β-D-glucose (N-acetylglucosamine), which is linked by β(1–4) glycosidic bonds found in nature [6]. Chitin is a rigid scaffold found in arthropod cuticle. Arthropods, include the crustaceans (e.g. crabs, lobsters, and other isopods), insects (e.g. wasps, bees, ants, beetles), arachnids (e.g. spiders, scorpions, ticks, mites), centipedes, millipedes and several lesser groups, account for approximately 80% of all known animal species [7]. Distribution of chitin is a widespread trait among both unicellular organisms (yeast, protists and diatoms) and invertebrates, from the first Metazoans (sponges) through the invertebrate (chordates) and up to fish [8]. In fungi chitin is the characteristic component of the taxonomical groups Zygo-, Asco-, Basidio- and Deuteromycetes [9]. Chitin can be directly drawn out in large quantities from crab, prawn shells and seafood wastes. *Penaeus monodon* (Fabricius, 1798) is a crustacean found in all coastal areas worldwide. The waste produced from shrimps is an emerging problem in countries such as India, where the food industry is based mainly on seafood [10]. In India, more than 1,00,000 tons of shrimp bio-waste is generated annually and only an insignificant amount of that bio-waste is utilized for the extraction of chitin while the rest is discarded or underutilized [11–14]. Therefore, extraction of economically important chitin from the shells of *P. monodon* (Fabricius, 1798) and its utilization in wastewater treatment are an additional source of income, which also reduces the problems created by shrimp waste. The application potential of chitin is multidimensional, such as in food and nutrition, material science, biotechnology, pharmaceuticals, agriculture and environmental protection [15]. The stability of chitin opens the way for the use of chitin as a template molecule for hydrothermal reactions and ultimately leads to the synthesis of advanced materials [16]. Synthesizing nanoparticles from chitin and chitosan enhances its application due to its larger surface area [17]. The aim of the present study was to investigate the CNP adsorption capability on three major industrial dyes, namely Methylene Blue (MB), Bromophenol Blue (BPB) and Coomassie Brilliant Blue (CBB). Efficacy of CNP over dye retention has been investigated at varied operating conditions such as pH, CNP dosage, contact time and initial dye concentration. The adsorption capability of CNP toward these dyes has been evaluated using Langmuir and Freundlich isotherms and their adsorption kinetics has been analyzed using pseudo first order and pseudo second order kinetic models. The chemical structure experimental dyes are presented in Fig. 1(a)–(c).

Material and methods

Materials

P. monodon (Fabricius, 1798) shells were collected from the Estuary of Southeast coast of Mandapam, Tamil Nadu, India. Sodium hydroxide, Acetone, Ethanol and Hydrochloric acid used were purchased from Sisco Research Laboratories Pvt. Ltd., Mumbai, India, and Dialysis membrane was purchased from HiMedia Laboratories, Mumbai, India. Methylene Blue, Bromophenol Blue and Coomassie Brilliant Blue were purchased from Sigma–Aldrich, USA.

Chitin nanoparticles isolation and characterization

Shells of *P. monodon* (Fabricius, 1798) were collected from the east coastal regions of (Mandapam) southern Tamil Nadu, India. The shells were washed in running tap water to remove the soluble organics, adherent proteins and other impurities. Washed shells were air dried at 25 ± 1 °C for 2 weeks. Dried shells were soaked in 0.5 M NaOH at 25 ± 1 °C for 24 h for the removal of proteins and lipids existing with shells. The NaOH was drained and the shells were washed with distilled water until the pH reaches neutral. The shells were again dried at 50 °C in a hot air oven for 48 h. Dried shells were ground as fine powder using a domestic blender and subjected to acid hydrolysis. The shells were soaked in 0.25 M HCl for 45 min and rinsed with distilled water until the pH reaches neutral. Again the sample was soaked in 2.5 M NaOH for 6 h at 80 °C and washed with distilled water until the pH reaches neutral. The alkali treatment was repeated twice and the remaining organic soluble compounds from the sample were removed by washing with acetone and ethanol thrice. The sample was dried for 10–15 days in hot air oven at 40 °C and white colored chitin was obtained.

CNP were isolated from the purified chitin by repeated acid hydrolysis [17]. Chitin powder was soaked in 3 M HCl for 1.5 h at 90 °C in a water bath. The sample was centrifuged at 6000 rpm for 10 min and the pellets were collected. The acid hydrolysis step was repeated thrice and the pellets were suspended in distilled water to dilute the acid concentration. The suspension was dialyzed against distilled water until it reaches pH 6 and was homogenized using a tissue homogenizer. The homogenized sample was collected and lyophilized at −60 °C to get the powder form of CNP. Mechanical disruption and ultrasonication were carried out to cut down the size of nanoparticles.

UV–Visible spectrophotometer was used to study the covalent and noncovalent interactions of a compound [18]. UV–Visible spectra of chitin were recorded in aqueous acid solution (0.1 M HCl) in a 1.0 cm Quartz cell at 25 ± 1 °C. The absorbance was measured using Shimadzu UV-2401 PC double beam spectrophotometer at the range between 190 and 500 nm range and 0.1 M HCl solution was used as control.

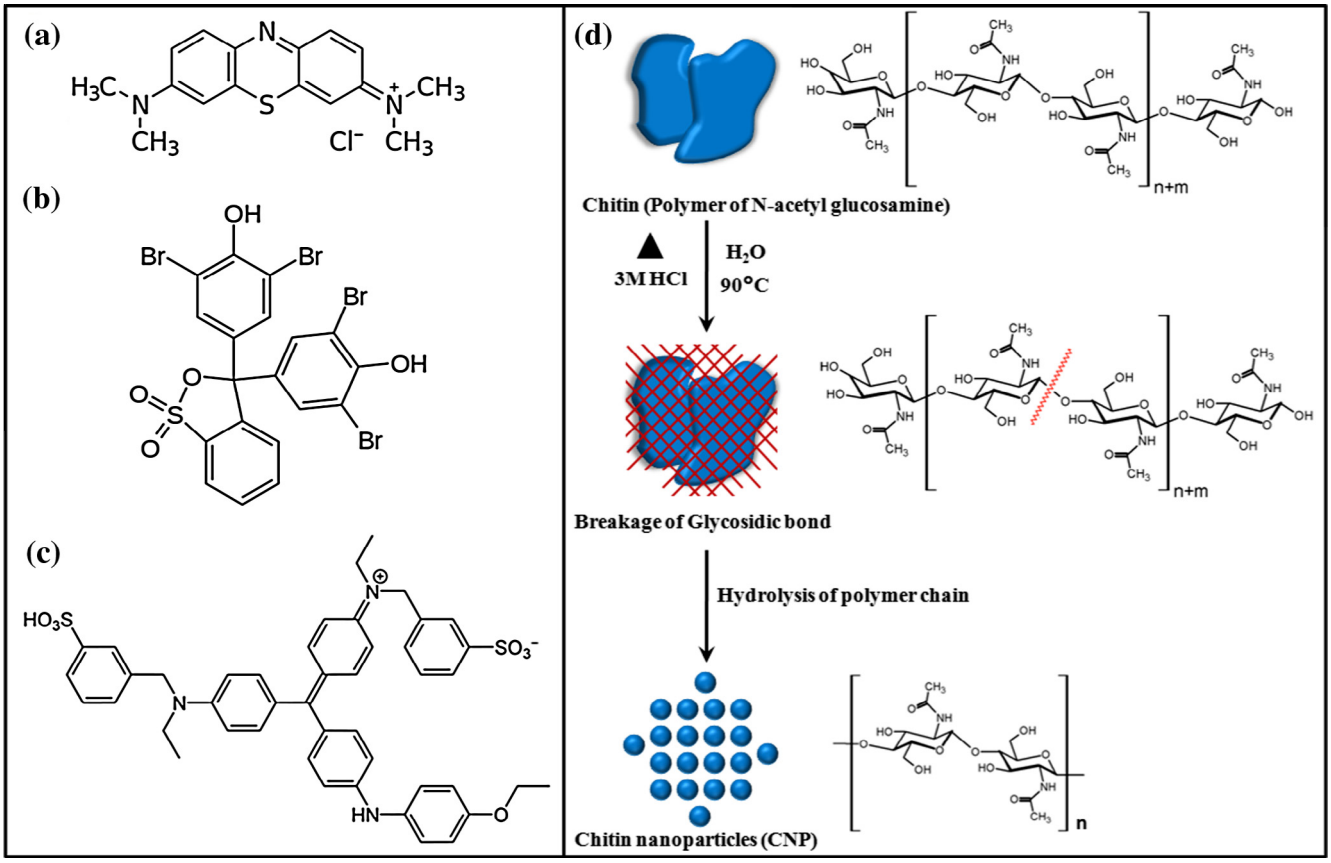

Fig. 1 Chemical structure of (a) MB, (b) BPB, (c) CBB and (d) Schematic diagram of CNP formation by acid hydrolysis.

Fourier transform infrared (FTIR) spectra of chitin and CNP were recorded with Nicolet 380 FTIR spectrometer. The sample was prepared at 0.25 mm thickness as KBr pellets (1 mg in 100 mg KBr) and stabilized under reactive humidity before acquiring the spectrum. The spectrum was measured between 400 and 4000 nm for 32 scans.

Solid state ^{13}C NMR spectrometer was used to analyze the magic angle spinning (MAS) of the sample (BRUKER DSX-300; BrukerBioSpin GmbH, Germany). Crosspolymerization MAS ^{13}C NMR spectrum of the sample was analyzed at 75 MHz, and the spinning rate was 9 kHz with a contact time of 0.0001 s and 5 s delay in between 2048 scans. CP-MAS NMR spectra were used to confirm the allomorphic nature and to estimate the degree of acetylation (DA) of the chitin and CNP. DA was calculated by dividing the resonance intensity of methyl group carbon by the average of glycosyl group carbons using the following equation [19]:

$$DA\% = CH_3I/[C_1I + C_2I + C_3I + C_4I + C_5I + C_6I] \times 100 \quad (1)$$

X-ray diffraction measurement on the powder sample was carried out (2 theta = 10–80° at 25 °C) using a diffractometer system (XPERT-PRO, PANalytical) equipped with Ni-filtered Cu K-Alpha1 radiation (k = 1.5406 Å). The diffractometer was operated with 0.47° divergent and receiving slits at 40 kV and 30 mA. A continuous scan was carried out with a step size of 0.05° two theta angle and a step time of 10.1 s. The crystalline index (I_{CR}) was calculated using the diffraction pattern with methods employed for diffraction studies of the polymers. Crystalline index was calculated using the intensities of the peaks at [1 1 0] lattice (maximum intensified peak) and at amorphous diffraction peak (am) by the following equation [20]:

$$I_{CR}\% = (I_{110} - I_{am})/I_{110} \times 100 \quad (2)$$

Thermo-gravimetric analysis of the chitin and CNP was done using Shimadzu TGA-Q500 instrument. About 4–6 mg of the sample was heated at 10 °C/min under nitrogen atmosphere (50 mL/min) in an interval of 20–900 °C.

Morphological examination of CNP was performed by High Resolution SEM. The sample was coated on copper grid and the microscopic analysis was conducted using a Quanta FEI 250, SEM operated at 10 kV.

Transmission Electron Microscopic (TEM) analysis was performed by dispersing the sample in milli-Q water, where one drop of the suspension was deposited in a carbon coated copper grid and allowed to air-dry. TEM imaging was performed using TECHNITE10 (Philips) under 80 kV power supply. Image analysis software ImageJ (National Institutes of Health, USA) was used to determine the size of the CNP.

Detection of particle size measurements of CNP was conducted using a Zetasizer Nano ZS DLS instrument (Malvern Instruments, Worcestershire, UK). The instrument used refractive index RI = 0.197, absorption = 3.090 and water as dispersant: temperature T = 25 °C, viscosity = 0.8872 cP, RI = 1.330 for measurements. The derived count rate, in kilo

counts per second (kcps) was recorded during particle size measurements.

Adsorption studies

Adsorption experiments were carried out as batch modes. Stock solution of the dyes was prepared and diluted with double distilled water. The pH of the dye solutions was adjusted using 0.1 N NaOH or 0.1 N HCl and obtained the desired pH (2–11). For each experiment, 15 mL of known dye solution was taken and 15 mg of CNP was added. The mixture was kept at 25 ± 1 °C and agitated at a constant speed (150 rpm/min). The samples were then collected and centrifuged at 7000 rpm for 10 min. The dye concentration in the supernatant was analyzed using a UV–Visible spectrometer. The absorbance at 668 nm (MB), 590 nm (BPB) and 580 nm (CBB) was used to calculate the equilibrium adsorption of the dyes. The percentage removal of dye was calculated using the following equation [21]:

$$\text{Percentage of removal} = ((C_0 - C_t)/C_0) \times 100 \quad (3)$$

where C_0 and C_t are the initial and final concentrations of dye before and after the adsorption in aqueous solution.

Quantity of adsorbed dyes at equilibrium was calculated using the following equation [22]:

$$q_e = (C_0 - C_t)v/w \quad (4)$$

where C_0 is the initial concentration (mg/L), C_t is the dye concentration at various time intervals (mg/L), v is the volume of experimental solution (mL) and w is the weight (g) of CNP.

Each experiment was performed in triplicate in identical conditions and the mean values were calculated.

Adsorption isotherms

Isotherms were used to express the relationship between the mass of dye adsorbed per unit mass of the adsorbent and the liquid phase dye concentration [23]. In the present investigation, two isotherm models, namely Langmuir and Freundlich isotherms have been adopted. The experimental data obtained from the effect of time interval in adsorption process were used to calculate the adsorption isotherms (Table 1).

Adsorption kinetics

The experimental data were investigated to study the adsorption process controlling system [24]. The pseudo first order and second order kinetic models were used and the experimental data obtained from the effect of time interval in adsorption process were used to calculate the kinetics (Table 1).

Table 1 Experimental conditions of isotherm and kinetic studies.

Dye	Dye concentration (mg/L)	pH	Temperature	CNP (mg)
MB	10	6	25 ± 1 °C	15
BPB	15	6	25 ± 1 °C	15
CBB	25	10	25 ± 1 °C	15

FTIR spectroscopy

Fourier transform infrared (FTIR) spectra of dyes, CNP, before and after adsorption were recorded with Nicolet 380 FTIR spectrometer. The samples are prepared as described previously (Chitin nanoparticles isolation and characterization).

Results and discussion

Chitin nanoparticle isolation and characterization

White color chitin power was obtained after deproteinization by NaOH, demineralization by HCl and removal of organic pigments using acetone and ethanol treatment of the shells. Further hydrolysis of chitin powder using HCl gives chitin nanoparticles. The sample was lyophilized in freeze-dryer and obtained the nanoparticles in powder form. In the present study, we used dried chitin powder as a precursor material for the preparation of chitin nanoparticles. Drying of chitin generates strong hydrogen bonds between fibers. Hence when treated with acid it forms nanoparticles instead of nanofibers. Series of chemical treatments and mechanical disintegration of shell wastes in wet condition give chitin nanofibers [25–27]. The mechanism of hydrolysis of chitin into CNP is shown in Fig. 1(d). The acid hydrolysis of chitin involves two main reactions namely depolymerization (hydrolysis of glycosidic bond) and deacetylation (breakdown of N-acetyl linkage), which was controlled by the concentration of acid used [28]. In the present study, 3 M HCl was used for the hydrolysis of chitin.

The UV–Visible spectrum of CNP exhibits the maximum absorption at 201 nm in 0.1 M HCl (Fig. 2(a)). According to Liu et al. [18] λ_{max} value for N-acetyl glucosamine (GlcNc) and glucosamine (GlcN) in 0.1 M HCl was 201 nm, which indicates that the monomer units present in the chitin were responsible for the observed λ_{max} value. In the present study, the absorbance was obtained at 201 nm indicating the presence of compounds namely N-acetyl glucosamine and glucosamine. Chitin and chitosan are having two chromophoric groups including GlcNc and GlcN. The extinction coefficient for wavelengths shorter than 225 nm was nonzero for these chromophoric groups. The monomer units GlcNc and GlcN contribute to the total absorbance of these polymers at a particular wavelength which indicates the absence of interaction existing within the chain [18].

FTIR spectrum of chitin and CNP is shown in Fig. 2(b). The spectra are typical polysaccharides and display a series of very sharp absorption peaks due to the crystallinity of the samples. The C═O stretching region of the amide, lies between 1600 and 1500 cm^{-1} [27]. The peak corresponds to amide I and yields different signatures for α-chitin and β-chitin. In this study, chitin shows a split amide peak at 1657 and 1630 cm^{-1}, likewise CNP show split amide I peak at 1659 and 1625 cm^{-1} and confirms the α allomorph. By contrast, β-chitin produces a single band for amide I [17]. The absence of peak at 1540 cm^{-1} confirmed that the chitin and CNP are free from proteins. The peaks for NH stretching present at 3267 cm^{-1} for chitin and 3264 cm^{-1} for CNP, also confirming the purity of the samples. The intra and inter-chain hydrogen bonds of chitin give peaks at 3445, 3267,

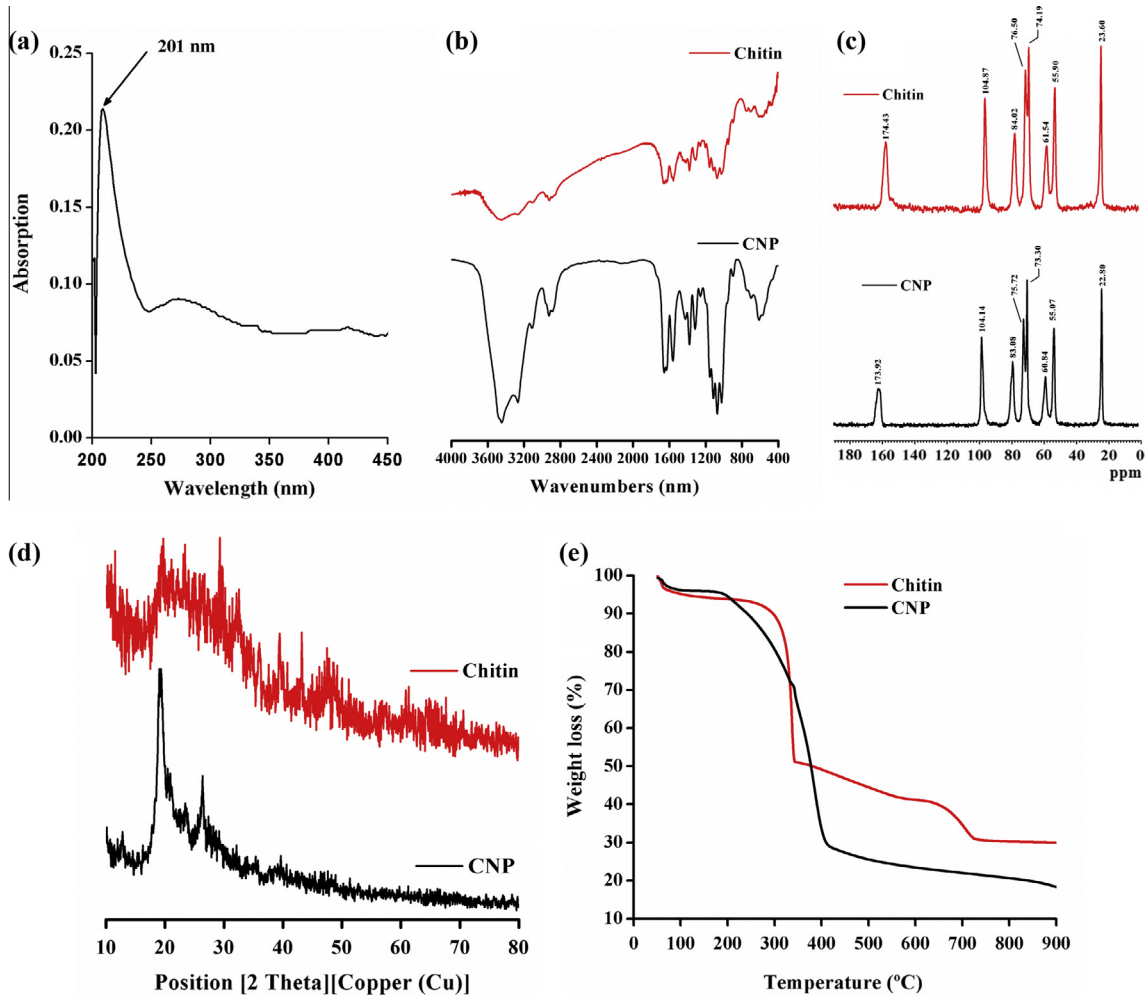

Fig. 2 (a) UV–Visible spectrum of CNP, (b) FTIR spectra of chitin and CNP, (c) ^{13}C Solid state CP-MAS spectra of chitin and CNP, (d) X-ray diffraction pattern of chitin and CNP and (e) thermo gravimetric analysis of chitin and CNP.

1657 cm^{-1} and CNP give peaks at 3444, 3264, 1659 cm^{-1}. Both chitin and CNP showed similar C-H bending at 1378 cm^{-1}. The strong peaks present in the carbonyl region (1760–1665 cm^{-1}) are characteristic peaks of α-chitin due to the stretching vibrations of C═O [29]. Hence the FTIR results confirmed that chitin and CNP are having same functional groups but showing shift in the peak value due to variation in DA and crystalline index.

CP-MAS ^{13}C NMR spectrum of the chitin and CNP is shown in Fig. 2(c). Eight signals were obtained for eight carbons of the GlcNc, which is a monomer unit of α-chitin. The spectrum of chitin gives a signal peak at 23.60 ppm for methyl group and C1–C6 carbons give signals at 104.87, 55.90, 76.50, 84.02, 74.19 and 61.54 ppm respectively. Chitin showed a signal for carbonyl group carbon at 174.43 ppm. Likewise the methyl group of CNP gives a signal at 22.80 ppm and C1−C6 carbons give signals respectively at 104.14, 55.07, 75.72, 83.08, 73.30 and 60.84 ppm. The carbonyl group of CNP produced a signal at 173.92 ppm. The C3 and C5 carbons produced separated signals at 6.50 and 74.19 for pure chitin, and at 75.72 and 73.30 ppm for CNP respectively. This separation indicates that the isolated chitin was in α-allomorph. Sajomsang and Gonil [30] have reported that the C3 and C5 signals have been clearly separated into two signals at 75.8 ppm and 73.5 ppm for α-chitin, while the C3 and C5 carbon signals have merged into a single resonance peak at 75 ppm for β-chitin. Cortizo et al. [31] also reported that the differences between the two polymorphs can be attributed to differences in the C3 and C5 configurations resulting from the hydrogen bonds. Very close spectra were also reported for α-chitin isolated from other sources such as bumble bee [32], shrimp [7], black coral [33] and cicada sloughs [30]. Signal assignments were made based on Tanner et al. [34].

The degree of acetylation was calculated using Eq. (1). The calculated DA for the isolated chitin and CNP were 95.61% and 96.8% respectively. Though during hydrolysis deacetylation occurred, the DA was higher than the starter chitin due to the reduction in the number of monomer units and removal of deacetylated monomers while washing with water. Degree of acetylation has varied based on the source organism, allomorphic nature and mode of isolation [35]. DA values of the chitin from cicada sloughs and the chitin from rice-field crab shells were 96.8 ± 0.1% and 97.5 ± 0.1%, respectively [36]. α-chitin has more DA value than that of β-chitin, as it has not been affected much during demineralization treatment. The high DA value of the CNP made it insoluble to most of

the common solvents when the DA was lower than 50% and becomes soluble in water under aqueous acidic conditions [37].

The diffraction pattern of the chitin and CNP has shown that five crystalline reflections in the 2θ range 4–40° (Fig. 2(d)). Highly intensified peak of the α-chitin has 2θ value 19.34 and *d*-spacing 4.58; also CNP have 2θ value 19.00° and *d*-spacing 4.62 nm. Similarly Joint Committee on Powder Diffraction Standards (JCPDS card no 351974) has also shown 2θ value 19.28° and *d*-spacing 4.60 nm for α-chitin. Diffraction pattern of chitin and CNP has shown similar crystalline reflections with the JCPDS.

Crystalline indices of chitin and CNP were calculated using Eq. (2), and were 79.04% and 83.73% respectively. In the present study, the DA decreases the crystalline index of chitin. Deacetylation of a polymer is known to decrease the crystalline index [38]. According to these results, size and DA influence the crystallinity of chitin. Stawski et al. [39] also reported that the crystallite size influences in the crystallization, crystalline perfection of chitin. Hence, chitin has low crystalline index than that of the CNP.

The TGA curve of chitin and CNP is shown in Fig. 2(e). In both curves the first stage of weight loss for chitin and CNP was 6.14% and 10.01% respectively at 60 °C. The second stage of weight loss for chitin occurs between 200 °C and 350 °C (42.86%); for CNP weight loss occurs between 240 °C and 450 °C (62.31%). The first stage is assigned to the loss of water because chitin has strong affinity toward water and therefore may be easily hydrated. The second stage corresponds to the thermal decomposition, vaporization and elimination of volatile compounds of chitin. In this study, third step corresponds to the remaining char and nonvolatile compounds. Al Sagheer et al. [35] observed similar decomposition TGA curve for chitin isolated from the marine sources. In the present study CNP have more thermal stability than starter chitin. The property was due to high DA and crystalline index of the CNP.

The morphology of CNP under scanning electron microscope is shown in Fig. 3(a). The micrograph of has showed dispersed particles with $\leqslant$50 nm in size with agglomerated morphology. The corresponding morphology of the particles may be due to the removal of some inorganic materials and proteins [30].

Transmission electron micrograph of the CNP is shown in Fig. 3(b). TEM microgram clearly indicates that the nanoparticles are approximately spherical in morphology and have agglomeration property. Nakorn [40] observed agglomeration with the particle size of 300 nm in nanowhiskers. In the present study, CNP formed after consecutive implementation of acidic hydrolysis and mechanical ultrasonication/disruption have the average particle size of 49 nm.

Dynamic light scattering of CNP and particle size distribution is depicted in Fig. 3(c). The particle size exhibited a distinct curve with average size of 115 nm. Contrastingly the TEM analysis shows average particle size of 49 nm. The increase in the particle size was due to the swelling and agglomeration property of chitin in aqueous solution. DA, hydrophobicity and the presence of amino group interacted with water are the limiting factors of swelling in chitin [41,42]. Kumar et al. [43] also reported that porosity and presence of ions in the aqueous solution may increase the swelling property and agglomeration of chitin.

Effect of pH on dye adsorption of CNP

pH plays an important role in aqueous chemistry and surface binding sites of the adsorbents. The effect of pH on the

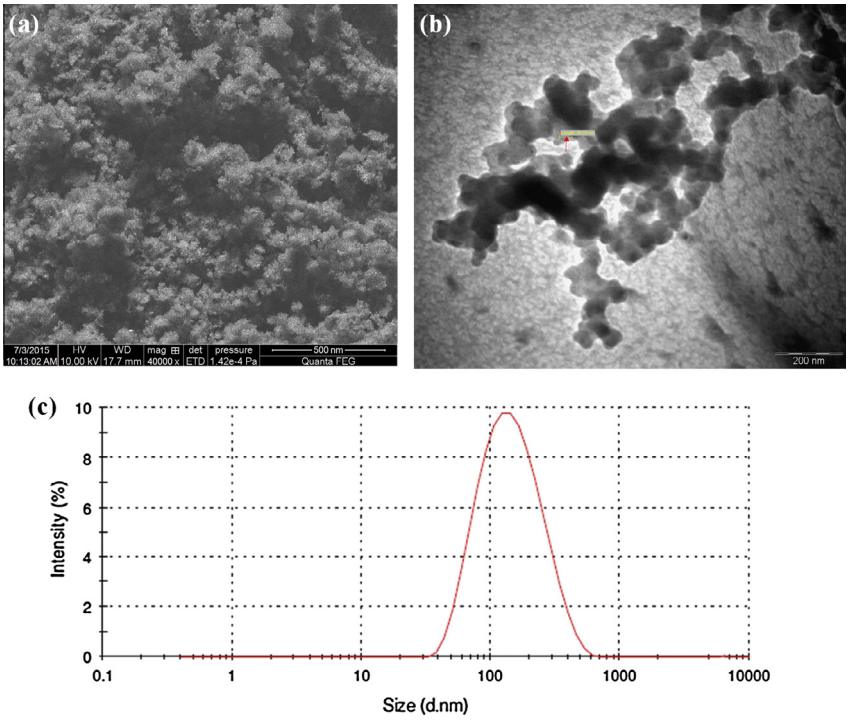

Fig. 3 (a) SEM micrograph of CNP at 40,000× magnification, (b) TEM micrograph of CNP at 93,000× magnification and (c) particle size distribution of CNP by dynamic light scattering.

adsorption of dyes in the range from 2 to 11 at 25 ± 1 °C with 15 mg CNP in 15 mL of aqueous dye solutions (MB – 10 mg/L, BPB – 15 mg/L and CBB – 25 mg/L) at a contact time of 30 min was investigated and the respective results are shown in Fig. 4(a). The percentage removal of dyes was calculated using Eq. (3) for all the operating parameters. The optimum pH of the dyes (MB, BPB and CBB) was 6, 5–6 and 10 respectively. The adsorption process achieved maximum at acidic pH for MB and BPB, whereas process achieved maximum at strong alkaline pH for CBB. MB is a cationic dye which is having strong positive charge. Chitin also has positive charge and point zero pH was 5.3. When there is a decrease in the pH below point zero pH the surface of the chitin becomes more positively charged, concentration of H^+ was high and they compete with MB cations for vacant adsorption sites causing a decrease in dye uptake. In this study the optimum pH for MB adsorption was 6, which is higher than the point zero pH. At this pH surface of chitin was negatively charged and the adsorption of MB was higher. Kushwaha et al. [44] also reported that the pH of the solution to be above the point zero, and the adsorbent surface was negatively charged and favors uptake of cationic dyes due to increased electrostatic force of attraction. In the case of BPB, pH influences the adsorption process very less. Percentage of adsorption at pH 2 was observed to be about 80.7%, whereas at pH 11 it is about 82.55% (Fig. 4(a)). For BPB, the maximum adsorption of 98.6% was observed at pH 6. Physical interactions such as formation of a hydrogen bond, van der Waals interactions, ion exchange and pore diffusion also influence the adsorption process [45]. By contrast, CBB shows maximum adsorption at pH 10. It appears that a change in pH of the solution results in the formation of different ionic species, and different CNP surface charges. The adsorption was low at lower pH even though the surface charge of the CNP was positive. This might have happened because of the zwitter ionic property of the dye as it gets aggregated themselves [46]. In addition, with increase in the pH the adsorption of CBB gets steadily increased and at pH 10 CBB shows maximum adsorption percentage.

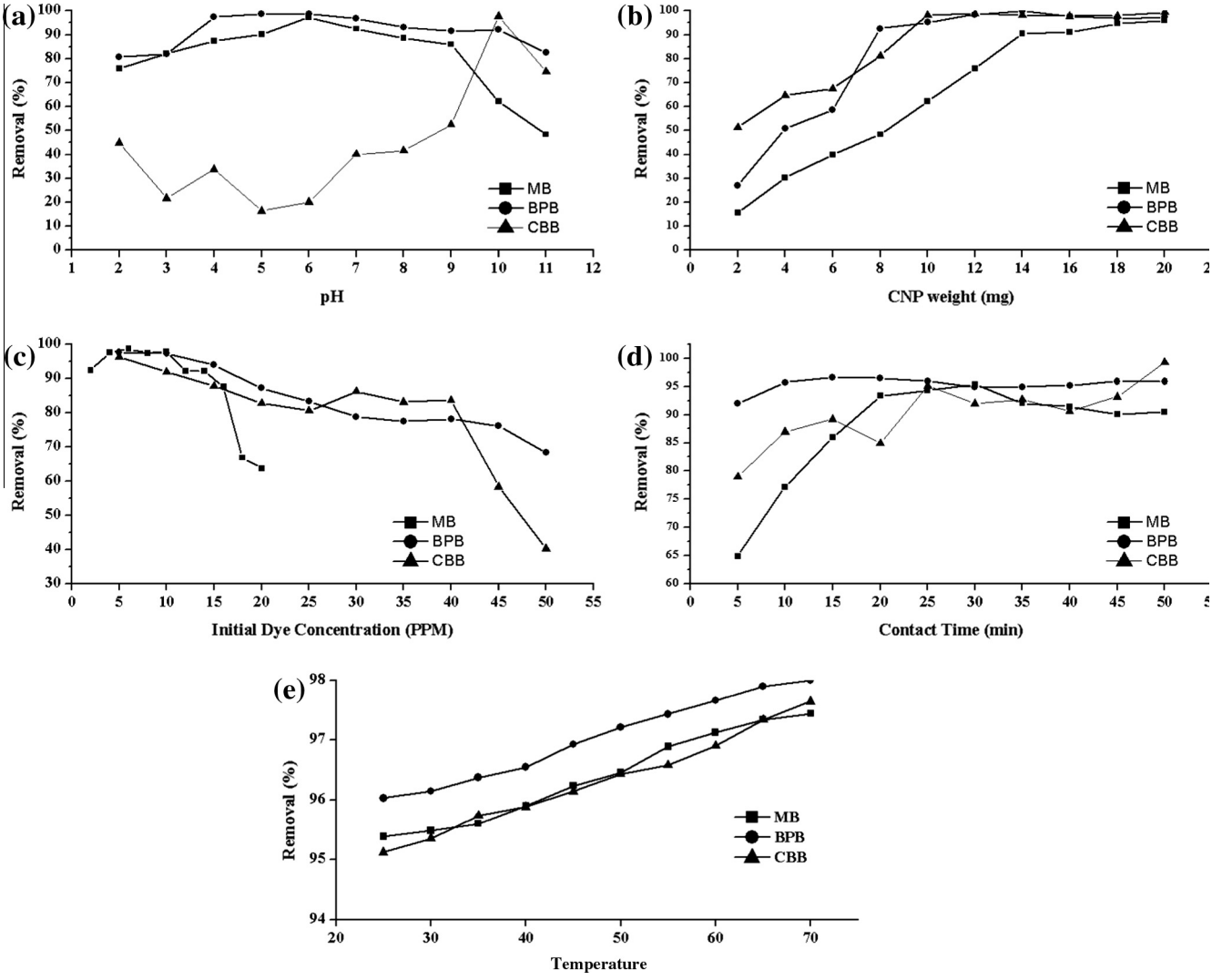

Fig. 4 Percentage removal of MB, BPB and CBB at (a) various pH, (b) various CNP concentration, (c) various initial dye concentration, (d) different contact time and (e) various temperature by CNP.

Effect of CNP concentration on dye adsorption

Fig. 4(b) shows the effect of CNP concentration in the adsorption process. By varying the CNP concentration between 2 and 20 mg at a constant initial dye concentration (MB – 10 mg/L, BPB – 15 mg/L and CBB – 25 mg/L) in 15 mL solution at a contact time of 30 min was studied. All these three dyes have shown similar results that the increase in concentration of CNP increases adsorption process. Percentage of adsorption increased from 15–95%, 27–96% and 51–99% for MB, BPB and CBB respectively. While there is an increase in the number of available adsorption sites the overall removal efficiency also gets increased [47]. Similarly in this study, increase in the concentration of CNP efficiently increases the adsorption process and 20 mg of CNP has adsorbed more than 95% of dyestuff in all the experimental dyes.

Effect of initial concentration of dyes on adsorption

The effect of various initial dye concentrations (2–20 mg/L for MB and 5–50 mg/L for BPB and CBB) on adsorption process at a fixed CNP dosage (15 mg/15 mL) and pH (6 for MB and BPB, 10 for CBB) for 30 min time interval was studied. An increase in the initial dye concentration leads to decrease in the adsorption process of the dyes (Fig. 4(c)). Due to increase in the concentration gradient between adsorbent and dyestuff, the percentage of removal was high until the system reaches its equilibrium. After equilibrium and saturation point, the dye stuff remains in the solution and the percentage of adsorption was decreased [48]. In this study, maximum adsorption was observed at 6 mg/L, 10 mg/L and 5 mg/L for MB, BPB and CBB respectively. While there is an increase in the dye concentration after equilibrium, a concentration gradient between the dyestuff and CNP was developed and the adsorption process was decreased.

Effect of contact time on dye adsorption of CNP

The effect of contact time on the adsorption at constant dye concentration (MB – 10 mg/L, BPB – 15 mg/L and CBB – 25 mg/L), pH (6 for MB and BPB, 10 for CBB) and 15 mg CNP at different time intervals (5–50 min) was studied and the results are shown in Fig. 4(d). The percentage removal of dyes increased dramatically in the initial stages, whereas, with increase of contact time the removal of dyes gradually gets increased until equilibrium. The optimum time taken to attain equilibrium was 30 min, 15 min and 25 min for MBB, BPB and CBB respectively. Moreover, within 5 min the percentage removal was obtained at 91% of CBB, 65% of MB and 79% of BPB by CNP. The adsorption rate was drastic in the initial contact time due to availability of the reactive site on the surface of the CNP [49]. Moreover, no significant changes were observed in the percentage of removal of the dyes after equilibrium. Similarly the percentage removal was constant after equilibrium due to the slow pore diffusion or saturation of adsorbent and the adsorption percentage was stable at higher time [49]. Contrary to other low cost adsorbent materials such as chitin hydrogels [23], sugarcane dust [50], neem sawdust [51], chaff [52], silica nano-sheets [53], *Caulerpa racemosa var. cylindracea* [54], silkworm exuviae [55], CNP show faster adsorption rate.

Effect of temperature on the dye adsorption of CNP

The effect of temperature on the adsorption at constant dye concentration (MB – 10 mg/L, BPB – 15 mg/L and CBB – 25 mg/L), pH (6 for MB and BPB, 10 for CBB) and 15 mg for 30 min time interval and the results are shown in Fig. 4(e). The result generally showed that the adsorption increased slightly with increase in temperature for all three dyes. This is characteristic of endothermic process and indicates that adsorption of dyes onto the chitin was enhanced at higher temperature. Similar results were reported in the adsorption of reactive red 141 [56], indigo carmine and trypan blue [57].

Adsorption isotherms

Langmuir adsorption isotherm

Langmuir isotherm model is the best known adsorption isotherm model for monolayer adsorption. The model can be represented as follows [58]:

$$C_e/q_e = (1/K_L q_m) + C_e/q_m \quad (5)$$

where q_e is the amount of dye adsorbed at equilibrium (mg/g); C_e is the concentration of dye at equilibrium (mg/L); q_m is the maximum adsorption capacity of dye per gram of adsorbent (mg/g); and K_L is the Langmuir constant (L/mg). q_e value of dyes was calculated using Eq. (4). The experimental data C_e/q_e were plotted against C_e (Fig. 5(a)). Langmuir constant K_L, and maximum adsorption per unit of the adsorbent (q_m) were calculated from the intercept and slope value of the plot. Correlation coefficient (R^2) was also calculated and the Langmuir parameters are listed in Table 1 for MB, BPB and CBB. Calculated R^2 value for MB, BPB and CBB were 0.992, 0.999 and 0.992 respectively. Further analysis of Langmuir equation was carried out, and dimensionless equilibrium parameter (R_L) was calculated. R_L is used as an indicator of adsorption experiment [47].

$$R_L = 1/(1 + K_L C_e) \quad (6)$$

where K_L is the Langmuir constant and C_e is the initial dye concentration. The value of R_L indicates the adsorption nature of the dye with the adsorbent. If the R_L value is >1, the adsorption process is unfavorable. Whether the R_L value is equal to 1 or the value lies in between 0 and 1 indicates that the adsorption is linear and favorable. $R_L = 0$ indicates irreversible adsorption process [47]. In the present investigation, R_L value for all the three dyes falls in between 0 and 1 and has confirmed that CNP are favorable for MB, BPB and CBB under the experimental conditions. The adsorption data were derived from the Langmuir equation and are listed in Table 2.

The maximum adsorption capacity (q_m) of CNP was compared with the reported by-products from the agricultural and industrial wastes assumed to be low-cost adsorbents and different dyes used are shown in Table 3. The hydrolyzation of polymer into nanoparticle form will change the physical properties of the material such as surface area and particle size [59]. This could be the reason for increase in the adsorption process. CNP show the better adsorption among these different biosorbents. Variation in adsorption capacity mainly attributed to the differences in experimental condition

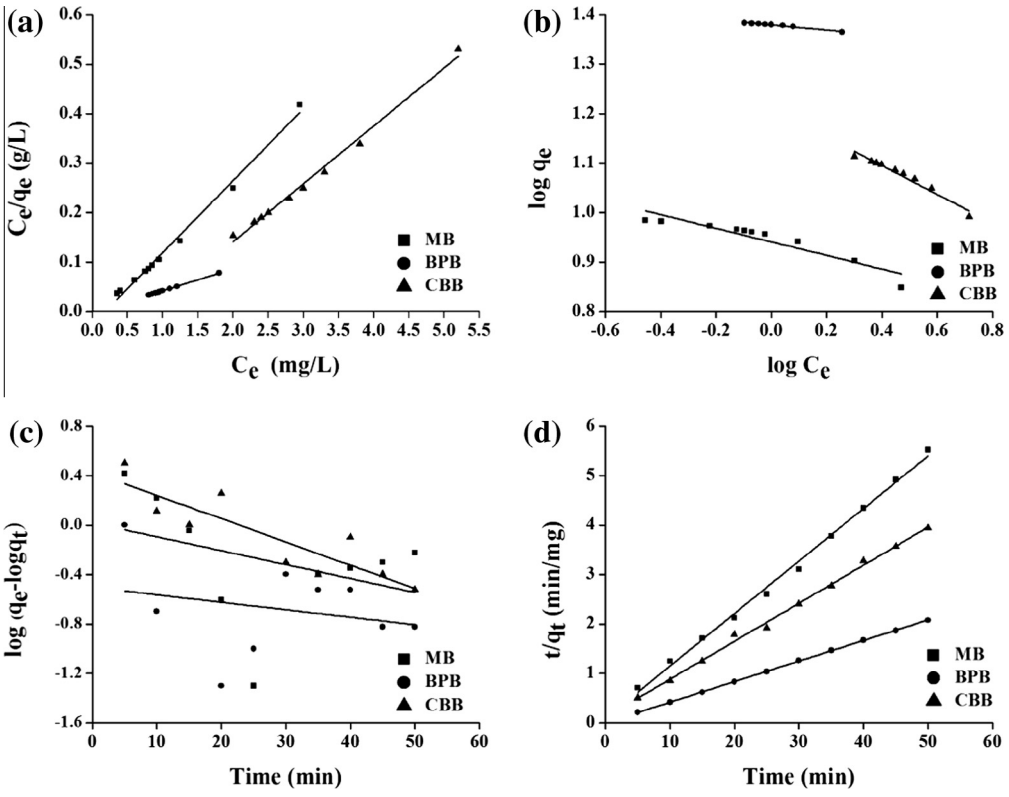

Fig. 5 (a) Langmuir isotherm, (b) Freundlich isotherm, (c) Pseudo first order kinetics and (d) Pseudo second order kinetic models for adsorption of MB, BPB and CBB onto CNP.

Table 2 Langmuir, Freundlich, pseudo first order and pseudo second order kinetics parameters for dye (MB, BPB, CBB) adsorption onto CNP.

Dye	Langmuir isotherm model				Freundlich isotherm model			Pseudo first order kinetics			Pseudo second order kinetics		
	q_m (mg/g)	K_L (L/mg)	R^2	R_L	K_F (L/mg)	$1/n$	R^2	k_1 (min^{-1})	q_e (mg/g)	R^2	k_2 (g/mg.min^{-1})	q_e (mg/g)	R^2
MB	6.900	0.027	0.992	0.599	0.940	0.137	0.875	0.010	0.040	0.119	0.086	9.434	0.996
BPB	22.720	0.003	0.999	0.930	1.380	0.052	0.981	0.000	1.360	0.124	0.001	24.390	0.999
CBB	8.550	0.093	0.992	0.395	1.212	0.290	0.964	0.018	0.435	0.722	0.113	13.158	0.996

conducted and properties of adsorbent such as the specific surface area, pore size and functional groups in biosorbents [48].

Freundlich absorption isotherm

Freundlich isotherm describes the heterogeneous system, reversible adsorption and not monolayer formation. Thereafter it has been assumed that once a dye molecule occupies a site, no further adsorption could take place at that site [23]. Freundlich isotherm equation is represented as follows:

$$\log q_e = \log K_F + (\log C_e)/n \quad (7)$$

where K_F and n are Freundlich constants.

The experimental data $\log q_e$ were plotted against $\log C_e$ to analyze the Freundlich isotherm (Fig. 5(b)). K_F (mg/g) is the Freundlich isotherm constant related to adsorption capacity and n is the Freundlich isotherm constant related to adsorption intensity which were calculated from the intercept and the slope value of the plot. When the $1/n$ value is between 0.1 and less than equal to 0.5 the adsorption process is wonderful. If the value is between 0.5 and 1 the process is easy to adsorb and if the value is greater than 1 it is difficult to adsorb [23]. In the present study $1/n$ value was closer to zero. Hence the adsorption process is more heterogeneous for all the three dyes. Correlation coefficient (R^2) was also calculated from the plot and the Freundlich parameters are listed in Table 2. When compared to Langmuir isotherm the R^2 values are low for Freundlich isotherm. The present study has shown that the CNP obey Langmuir isotherm for MB, BPB and CBB.

Adsorption kinetics

Pseudo first order kinetics

The pseudo first order kinetics are represented as follows [24]:

$$\log(q_e - q_t) = \log q_e - (k_1 t/2.303) \quad (8)$$

where q_e and q_t indicate the amount of dye adsorbed at equilibrium and at a specific time (mg/g) and k_1 (min^{-1}) is the first order rate constant. First order rate constant k_1 was calculated

Table 3 Comparison of the maximum adsorption of CNP and various adsorbents with different dyestuff.

Adsorbent	Dye	q_m (mg/g)	Sources
Sugarcane dust	Crystal violet	3.80	[50]
Neem sawdust	Crystal violet	3.80	[51]
Chaff	MB	30.70	[52]
Silica nano-sheets	MB	12.66	[53]
Caulerpa racemosa var. cylindracea	MB	5.23	[54]
Silkworm exuviae	MB	29.54	[55]
Chitin hydrogels	Malachite green	0.10	[23]
CNP	MB	6.90	Present study
CNP	BPB	22.72	Present study
CNP	CBB	8.55	Present study

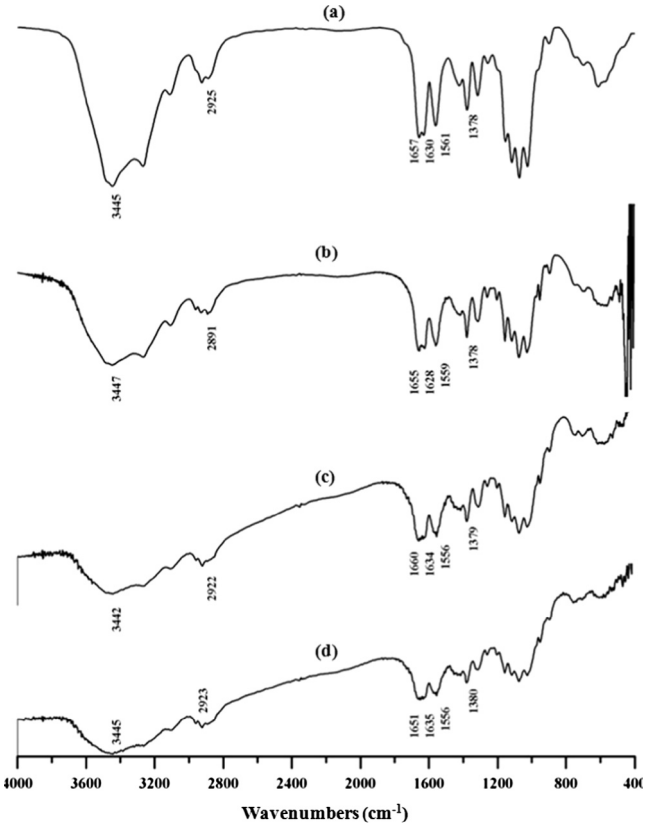

Fig. 6 FTIR spectrum of CNP (a) before and after (b) MB (c) BPB (d) CBB adsorption.

Table 4 Peaks of CNP and shifting of peak values (nm) after adsorption of CBB, BPB and CBB.

Vibration modes	CNP	CNP–MB	CNP–BPB	CNP–CBB
O—H stretching vibration	3445	3447	3442	3445
Amide 1	1657	1655	1660	1651
Amide 1	1630	1628	1634	1635
Amide 2	1561	1559	1556	1556
C—H stretching	2925	2891	2922	2923
C—H bending	1378	1378	1379	1380

from the slope value of the linear plot of log $(q_e - q_t)$ versus t. Correlation coefficient (R^2) was also calculated from the plot (Fig. 5(c)). Pseudo first order parameters are listed in Table 2.

Pseudo second order kinetics

The pseudo second order kinetics equation is as follows [24]:

$$t/q_t = 1/(k_2 q_e^2) + t/q_e \quad (9)$$

k_2 (g/mg min) is the second order rate constant.

Experimental data t/q_t were plotted against t (Fig. 5(d)) and calculated the pseudo second order constant K_2 and equilibrium adsorption capacity of CNP q_e from the intercept and slope value. Second order kinetic parameters are listed in Table 2. Correlation coefficient (R^2) was also calculated from the plot. The shape of the line determines which kinetic model fit for the adsorption process [48]. The R^2 values for MB, BPB and CBB were 0.996, 0.999 and 0.996 respectively. R^2 value indicates that the adsorption process fits better with second order kinetics rather than first order kinetics.

FTIR analysis of dye adsorption onto CNP

FTIR spectrum (Fig. 6) was used to analyze the changes in functional groups of CNP after the adsorption of dyestuff. The shifting of peaks after adsorption of dyestuff with CNP is listed in Table 4. Significant changes were observed in the peak values, which indicate the existence of physical interaction between CNP and the dyestuff. Dolphen and Thiravetyan [59] have reported similar shifting phenomenon with the adsorption of melanoidins by chitin fibers and have also stated that the shifting was due to electrostatic and chemical adsorption. When malachite green was adsorbed using chitin hydrogels, similar shifting was recorded by Tang et al. [23].

Conclusions

α-Chitin nanoparticles from the shells of *P. monodon* (Fabricius, 1798) were found to be a promising material for the purification of water dyestuff contamination. The prepared CNP have 49 nm average particle size with 96.8% DA and 83.73% crystallinity. The experiments done at various physical parameters have showed that CNP adsorb dyes in a very short period of exposure in normal environmental conditions and do not need any specific conditions for the adsorption process. The experimental data were analyzed using Langmuir,

Freundlich isotherms, pseudo first and second order kinetics. By comparing the correlation coefficient determined for each linear transformation of isotherm analysis, the Langmuir isotherm was found to be the best prediction for the adsorption of MB, BPB and CBB from aqueous solutions. The results showed that adsorption of MB, BPB and CBB on CNP fitted better to the pseudo second order kinetics rather than the pseudo first order kinetics. The reaction mechanism of adsorption was due to physical adsorption occurring between the dyestuff and the CNP. The shells of *P. monodon* (Fabricius, 1798) provide a renewable material and could be acquired from shrimp farms to ensure a sustainable use of the waste material. CNP are a simple, fast reacting, low cost biodegradable materials that can be as used for effective environmental protection.

Conflict of interest

The authors have declared no conflict of interest.

Compliance with Ethics Requirements

This article does not contain any studies with human or animal subjects.

Acknowledgments

The financial support from University Grants Commission, Govt. of India (40-389/2011(SR)) is gratefully acknowledged. The authors also thank Indian Institute of Science Bangalore, Indian Institute of Technology Madras and Veterinary University, Chennai, for providing instrumental support.

References

[1] Lin S, Lin C. Treatment of textile waste effluents by ozonation and chemical coagulation. Water Res 1993;27(12):1743–8.
[2] Ganesh R, Boardman G, Michelsen D. Fate of azo dyes in sludges. Water Res 1994;28(6):1367–76.
[3] McKay G. Analytical solution using a pore diffusion model for a pseudo irreversible isotherm for the adsorption of basic dye on silica. AIChE J 1984;30:692–7.
[4] Kavitha D, Namasivayam C. Experimental and kinetic studies on methylene blue adsorption by coir pith carbon. Bioresour Technol 2007;98(1):14–21.
[5] Ciesielczyk F, Bartczak P, Wieszczycka K, Siwińska-Stefańska K, Nowacka M, Jesionowski T. Adsorption of Ni(II) from model solutions using co-precipitated inorganic oxides. Adsorption 2013;19(2–4):423–34.
[6] Dutta PK, Ravikumar MNV, Dutta J. Chitin and chitosan for versatile applications. J Macromol Sci Part C Polym Rev 2002;42(3):307–54.
[7] Ehrlich H. Chitin and collagen as universal and alternative templates in biomineralization. Int Geol Rev 2010;52(7–8):661–99.
[8] Wysokowski M, Bazhenov VV, Tsurkan MV, Galli R, Stelling AL, Stöcker H, et al. Isolation and identification of chitin in three-dimensional skeleton of *Aplysina fistularis* marine sponge. Int J Biol Macromol 2013;62:94–100.
[9] Muzzarelli RA, Boudrant J, Meyer D, Manno N, DeMarchis M, Paoletti MG. Current views on fungal chitin/chitosan, human chitinases, food preservation, glucans, pectins and inulin: a tribute to Henri Braconnot, precursor of the carbohydrate polymers science, on the chitin bicentennial. Carbohydr Polym 2012;87(2):995–1012.
[10] Wysokowski M, Klapiszewski , Moszyński D, Bartczak P, Szatkowski T, Majchrzak I, et al. Modification of chitin with kraft lignin and development of new biosorbents for removal of cadmium(II) and nickel(II) ions. Mar Drugs 2014;12(4):2245–68.
[11] Mathew P, Nair KGR. Ensilation of shrimp waste by *Lactobacillus fermentum*. Fish Technol 2006;43:59–62.
[12] Suresh PV, Anil Kumar PK, Sachindra NM. Thermoactive b-N-acetylhexosaminidase production by a soil isolate of Penicillium monoverticillium CFR 2 under solid state fermentation: parameter optimization and application for N-acetyl chitooligosaccharides preparation from chitin. World J Microbiol Biotechnol 2011;27:1435–47.
[13] Suresh PV, Sachindra NM, Bhaskar N. Solid state fermentation production of chitin deacetylase by *Colletotrichum lindemuthianum* ATCC 56676. J Food Sci Technol 2011;48(3):349–56.
[14] Suresh PV, Anil Kumar PK. Enhanced degradation of a-chitin materials prepared from shrimp processing byproduct and production of N-acetyl-D-glucosamine by thermoactive chitinases from soil mesophilic fungi. Biodegradation 2012;23, 597-7.
[15] Anitha A, Sowmya S, Kumar PS, Deepthi S, Chennazhi KP, Ehrlich H, et al. Chitin and chitosan in selected biomedical applications. Prog Polym Sci 2014;39(9):1644–67.
[16] Wysokowski M, Motylenko M, Stöcker H, Bazhenov VV, Langer E, Dobrowolska A, et al. An extreme biomimetic approach: hydrothermal synthesis of β-chitin/ZnO nanostructured composites. J Mater Chem B Mater Biol Med 2013;1(46):6469–76.
[17] Goodrich JD, Winter WT. α-Chitin nanocrystals prepared from shrimp shells and their specific surface area measurement. Biomacromolecules 2007;8:252–7.
[18] Liu D, Wei Y, Yao P, Jiang L. Determination of the degree of acetylation of chitosan by UV spectrophotometry using dual standards. Carbohydr Res 2006;341:782–5.
[19] Ottey MH, Varum KH, Smidsrod O. Compositional heterogeneity of heterogeneously deacetylated chitosans. Carbohydr Polym 1996;29(1):17–24.
[20] Focher B, Beltrame PL, Naggi A, Torri G. Alkaline N-deacetylation of chitin enhanced by flash treatments, reaction kinetics and structure modifications. Carbohydr Polym 1996;12(4):405–18.
[21] Mundhe KS, Gaikwad AB, Torane RC, Deshpande NR, Kashalkar RV. Adsorption of methylene blue from aqueous solution using *Polyalthia longifolia* (Ashoka) seed powder. J Chem Pharm Res 2012;4(1):423–36.
[22] Sun L, Wana S, Luo W. Biochars prepared from anaerobic digestion residue, palm bark, and eucalyptus for adsorption of cationic methylene blue dye: characterization, equilibrium, and kinetic studies. Bioresour Technol 2013;140:406–13.
[23] Tang H, Zhou W, Zhang L. Adsorption isotherms and kinetics studies of malachite green on chitin hydrogels. J Hazard Mater 2012;209–210:218–25.
[24] Gurusamy A, Lai YL, Jiunn-F L. Adsorption of reactive dye from an aqueous solution by chitosan: isotherm, kinetic and thermodynamic analysis. J Hazard Mater 2008;152:337–46.
[25] Ifuku S. Chitin and chitosan nanofibers: preparation and chemical modifications. Molecules 2014;19(11):18367–80.
[26] Nata IF, Wang SSS, Wu TM, Lee CK. *β*-Chitin nanofibrils for self-sustaining hydrogels preparation via hydrothermal treatment. Carbohydr Polym 2012;90(4):1509–14.
[27] Lu Y, Sun Q, She X, Xia Y, Liu Y, Li J, Yang D. Fabrication and characterisation of α-chitin nanofibers and highly

transparent chitin films by pulsed ultrasonication. Carbohydr Polym 2013;98(2), 1497–104.
[28] Einbu A, Vårum KM. Depolymerization and de-N-acetylation of chitin oligomers in hydrochloric acid. Biomacromolecules 2007;8(1):309–14.
[29] Gopalan Nair K, Dufresne A. Crab shell chitin whisker reinforced natural rubber nanocomposites. 1. Processing and swelling behavior. Biomacromolecules 2003;4(3):657–65.
[30] Sajomsang W, Gonil P. Preparation and characterization of α-chitin from Cicada Sloughs. Mater Sci Eng C 2010;30:357–63.
[31] Cortizo MS, Berghoff CF, Alessandrin JL. Characterization of chitin from *Illex argentinus* squid pen. Carbohydr Polym 2008;74:10–5.
[32] Majtan J, Bılikova K, Markovic O, Grof J, Kogan G, Simuth J. Isolation and characterization of chitin from bumblebee *Bombusterrestris*. Int J Biol Macromol 2007;40:237–41.
[33] Bo M, Bavestrello G, Kurek D. Isolation and identification of chitin in the black coral Parantipatheslarix *Anthozoa: Cnidaria*. Int J Biol Macromol 2012;51:129–37.
[34] Tanner SF, Chanzy H, Vincendon M, Roux JC, Gaill F. High-resolution solid-state carbon-13 nuclear magnetic resonance study of chitin. Macromolecules 1990;23:3576–83.
[35] Al Sagheer FA, Al-Sughayer MA, Muslim S, Elsabee MZ. Extraction and characterization of chitin and chitosan from marine sources in Arabian Gulf. Carbohydr Polym 2009;77:410–9.
[36] Gonil P, Sajomsang W. Applications of magnetic resonance spectroscopy to chitin from insect cuticles. Int J Biol Macromol 2012;51(4):514–22.
[37] Kasaai MR. Determination of the degree of N-acetylation for chitin and chitosan by various NMR spectroscopy techniques: a review. Carbohydr Polym 2010;79:801–10.
[38] Pacheco N, Garnica-Gonzalez M, Gimeno M, Bárzana E, Trombotto S, David L, Shirai K. Structural characterization of chitin and chitosan obtained by biological and chemical methods. Biomacromolecules 2011;12(9):3285–90.
[39] Stawski D, Rabiej S, Herczyńska L, Draczyński Z. Thermogravimetric analysis of chitins of different origin. J Therm Anal Calorim 2008;93(2):489–94.
[40] Nakorn PNA. Chitin nanowhisker and chitosan nanoparticles in protein immobilization for biosensor applications. J Met Mater Miner 2008;18(2):73–7.
[41] Shelma R, Paul W, Sharma CP. Chitin nanofibre reinforced thin chitosan films for wound healing application. Trends Biomater Artif Org 2008;22:111–5.
[42] Baskar D, Kumar TS. Effect of deacetylation time on the preparation, properties and swelling behavior of chitosan films. Carbohydr Polym 2009;78(4):767–72.
[43] Kumar PS, Abhilash S, Manzoor K, Nair SV, Tamura H, Jayakumar R. Preparation and characterization of novel β-chitin/nanosilver composite scaffolds for wound dressing applications. Carbohydr Polym 2010;80(3):761–7.
[44] Kushwaha AK, Gupta N, Chattopadhyaya MC. Removal of cationic methylene blue and malachite green dyes from aqueous solution by waste materials of *Daucus carota*. J Saudi Chem Soc 2014;18(3):200–7.
[45] Iqbal J, Wattoo FH, Wattoo MHS, Malik R, Tirmizi SA, Imran M, Ghangro AB. Adsorption of acid yellow dye on flakes of chitosan prepared from fishery wastes. Arab J Chem 2011;4(4):389–95.
[46] Guo Y, Zhao J, Zhang H, Yang S, Qi J, Wang Z, Xu H. Use of rice husk-based porous carbon for adsorption of Rhodamine B from aqueous solutions. Dyes Pigm 2005;66(2):123–8.
[47] Kumar M, Bijay PT, Vinod KS. Crosslinked chitosan/polyvinyl alcohol blend beads for removal and recovery of Cd(II) from wastewater. J Hazard Mater 2009;172:1041–8.
[48] El-Sayed GO. Removal of methylene blue and crystal violet from aqueous solutions by Palm Kernel Fiber. Desalination 2011;272:225–32.
[49] Rodríguez AJM, Mazzoco RR. Adsorption studies of methylene blue and phenol onto black stone cherries prepared by chemical activation. J Hazard Mater 2010;180(1–3):656–61.
[50] Khattri SD, Singh MK. Colour removal from dye wastewater using sugar cane dust as an adsorbent. Adsorpt Sci Technol 1999;17, 269–2.
[51] Khattri SD, Singh MK. Colour removal from synthetic dye wastewater using a bioadsorbent. Water Air Soil Pollut 2000;120(3–4):283–94.
[52] Han R, Wang Y, Han P, Shi J, Yang J, Lu Y. Removal of methylene blue from aqueous solution by chaff in batch mode. J Hazard Mater 2006;137(1):550–7.
[53] Zhao M, Tang Z, Liu P. Removal of methylene blue from aqueous solution with silica nano-sheets derived from vermiculite. J Hazard Mater 2008;158(1):43–51.
[54] Cengiz S, Cavas L. Removal of methylene blue by invasive marine seaweed: *Caulerparacemosa* var. cylindracea. Bioresour Technol 2008;99(7):2357–63.
[55] Chen H, Zhao J, Dai G. Silkworm exuviae – a new non-conventional and low-cost adsorbent for removal of methylene blue from aqueous solutions. J Hazard Mater 2011;186(2–3):1320–7.
[56] Dolphen R, Sakkayawong N, Thiravetyan P, Nakbanpote W. Adsorption of Reactive Red 141 from wastewater onto modified chitin. J Hazard Mater 2007;145(1):250–5.
[57] Akkaya G, Uzun İ, Güzel F. Adsorption of some highly toxic dyestuffs from aqueous solution by chitin and its synthesized derivatives. Desalination 2009;249(3):1115–23.
[58] Huanga XY, Bub HT, Jianga GB, Zeng MH. Cross-linked succinyl chitosan as an adsorbent for the removal of Methylene Blue from aqueous solution. Int J Biol Macromol 2011;49:643–51.
[59] Dolphen R, Thiravetyan T. Adsorption of melanoidins by chitin nanofibers. Chem Eng J 2011;166:890–5.